Supplement of Geosci. Model Dev., 17, 4181–4197, 2024
https://doi.org/10.5194/gmd-17-4181-2024-supplement

Geoscientific Model Development
Open Access
EGU

Supplement of

Importance of microphysical settings for climate forcing by stratospheric SO_2 injections as modeled by SOCOL-AERv2

Sandro Vattioni et al.

Correspondence to: Sandro Vattioni (sandro.vattioni@env.ethz.ch) and Andrea Stenke (andrea.stenke@env.ethz.ch)

S1 Summary of sulfur burdens and fluxes

Table S1 summarizes numerical results of sulfur burdens and fluxes for most of the simulations performed in this study. Simulations names are the same as in Table 1. In addition, the index "_no_interp." refers to the old representation of passing the H_2SO_4 produced from the gas-phase chemistry routine to the microphysics module in one go, rather than splitting it properly among the N_{micro} substeps.

Table S1. Global total and stratospheric aerosol burden ($\mathrm{Gg(S)}$), as well as stratospheric sulfur fluxes between condensed and gas phase due to nucleation, condensation and evaporation ($\mathrm{Gg(S)\,yr^{-1}}$). The net cross-tropopause flux of sulfate aerosol ($\mathrm{Gg(S)\,yr^{-1}}$) is calculated by balancing the stratospheric sulfur fluxes between condensed and gas phase, assuming the stratospheric aerosol burden to be in equilibrium.

Simulation name	Total burden	Stratospheric burden	Nucleation	Condensation	Evaporation	Net cross-tropopause
BG_CN_20_no_interp.	708.8	167.7	29.9	82.7	5.9	106.7
BG_CN_20	704.4	164.6	1.4	113.1	5.3	109.2
BG_NC_20_no_interp.	709.1	165.7	32.0	80.9	4.9	108.0
BG_NC_20	705.4	166.1	9.6	109.0	5.8	112.8
S5_CN_20	4582.0	3710.9	1.8	5076.3	4.6	5073.5
S5_CN_200	4787.3	3916.4	78.2	5005.8	5.5	5078.5
S5_NC_20	4825.2	3954.7	532.4	4549.1	5.9	5075.6
S5_NC_200	4788.0	3924.2	113.9	4967.8	5.6	5076.1
S25_CN_20	16699.6	14663.5	1.9	25050.1	4.1	25047.9
S25_CN_200_no_interp.	18687.9	16667.5	9138.8	15572.3	4.6	24706.5
S25_CN_200	18423.3	16396.8	102.1	24951.5	4.2	25049.4
S25_NC_20	22309.2	20296.3	11345.9	14152.5	447.2	25051.2
S25_NC_200_no_interp.	18865.9	16840.9	21090.5	3623.2	7.2	24706.5
S25_NC_200	18610.1	16587.2	331.7	24725.6	4.0	25053.3
S25_NC_60	18694.9	16677.8	1086.9	23965.0	4.1	25047.8
BG_CN_20 (SOCOLv4)	432	150	10	110	10	110
S5p_CN_20 (SOCOLv4)	4875	4240	10	4960	20	4970
S5p_NC_20 (SOCOLv4)	5907	5290	4290	840	180	4950

S2 Importance of proper treatment of gasphase H_2SO_4 concentrations

In previous versions of SOCOL-AER the total amount of H_2SO_4 molecules produced by the chemistry scheme, which is called every two hours, was directly passed to the microphysical loop. The gaseous H_2SO_4 concentration was then consecutively updated by condensation and nucleation. This approach leads to an artificial spike in H_2SO_4 concentrations and supersaturations each time at the beginning of the microphysical calculation, which then gradually decreased over the microphysical loop. In reality, however, chemical H_2SO_4 production as well as nucleation and condensation occur continuously, resulting in a smoother evolution of atmospheric H_2SO_4 supersaturations. Therefore, it is important to distribute the chemical H_2SO_4 production uniformly among the N_{micro} substeps, in particular under high sulfur conditions. This is done by updating the gasphase H_2SO_4 concentration by the term $\Delta\ H_2SO_4/N_{\mathrm{micro}}$ after each microphyiscal substep, with $\Delta\ H_2SO_4 = H_2SO_{4\mathrm{afterchemistry}} - H_2SO_{4\mathrm{beforechemistry}}$ being the total amount of chemically produced H_2SO_4 molecules produced in one chemical timestep (Fig. 1). This avoids erroneously large H_2SO_4 concentrations at the beginning of the microphyiscal loop.

Figure S1 compares the resulting size distributions for the model versions with and without (_no_interp.) interpolation of the chemical H_2SO_4 production with $N_{\mathrm{micro}} = 200$. In the _no_interp. case, the gas-phase H_2SO_4 reaches its equilibrium vapor pressure through nucleation and condensation within the first few iterations of N_{micro}. During the remaining iterations of N_{micro} coagulation is the only process influencing the size distribution. This results in a peak in the nucleation mode around 3 nm and in higher number concentrations below 0.3 $\mu\mathrm{m}$ compared with S25_NC_200. The new setup which accounts for the interpolation of H_2SO_4 production within the microphyiscal subloop, however, results in more reasonable nucleation and condensation rates in which the nucleation mass flux is only 1-4 % of the condensation mass flux (see Table S1). The new treatment of the gas-phase H_2SO_4 is especially important when dealing with high H_2SO_4 supersaturations, but has no significant effect under background conditions (see BG simulations in Table S1). All the data presented in this paper account for the interpolation of H_2SO_4 production within the microphysical subloop.

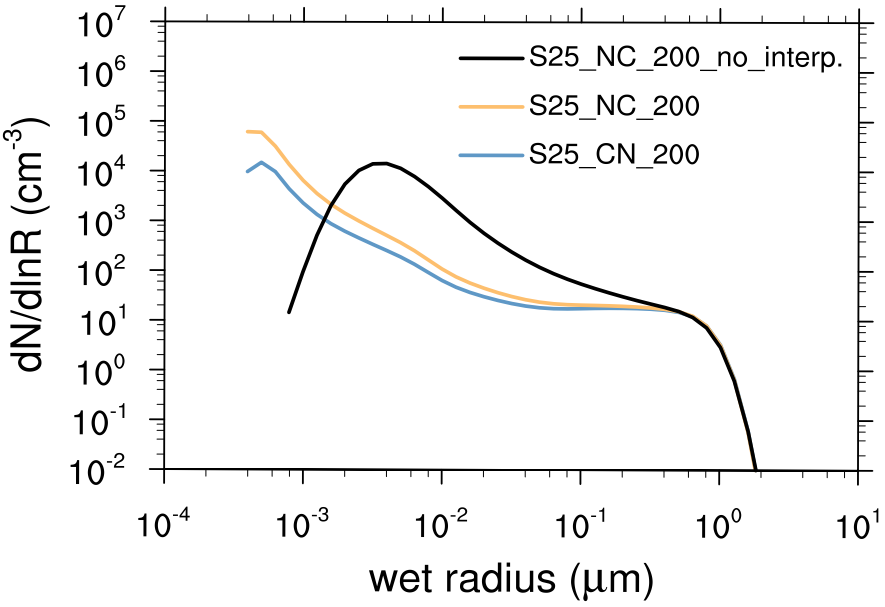

Figure S1. Size distributions ($dN/d\ln R$, $\mathrm{particles\,cm^{-3}}$) averaged between 30°S and 30°N at 55 hPa for the model simulations with regional SO_2 injections of 25 $\mathrm{Tg(S)\,yr^{-1}}$. While the blue and orange curves show the convergence of the size distribution when interpolating the H_2SO_4 molecules produced during the 2h-chemical timestep equally over N_{micro}, the black curve shows the resulting size distribution when passing the produced H_2SO_4 molecules to the microphysical subloop in one go.

S3 Influence of settings on aerosol surface area density

Climate intervention by stratospheric SO_2 emission yields an increase in aerosol burden and, thus, to a larger surface area density (SAD) available for heterogeneous chemistry. The SAD does not only depend on the total burden, but also on the detailed size distribution, as smaller particles have a greater surface area per unit mass.

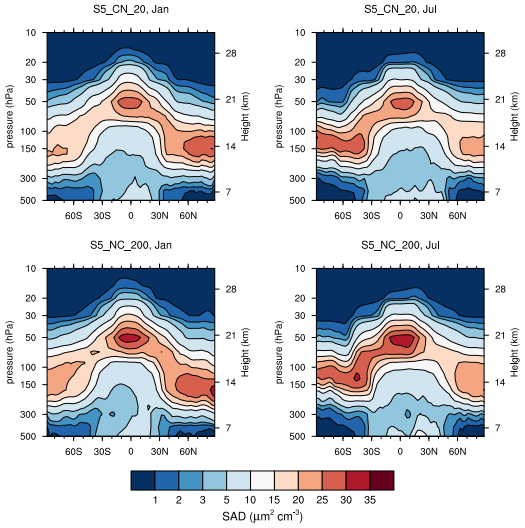

Figure S2. Zonal mean surface area density ($\mu m^2 cm^{-3}$) for January (left) and July (right) for the model simulations with 5 Tg(S) yr^{-1}. Top: S5_CN_20, i.e. the original setting in SOCOL-AER biased towards condensation. Bottom: the unbiased S5_NC_200 setting.

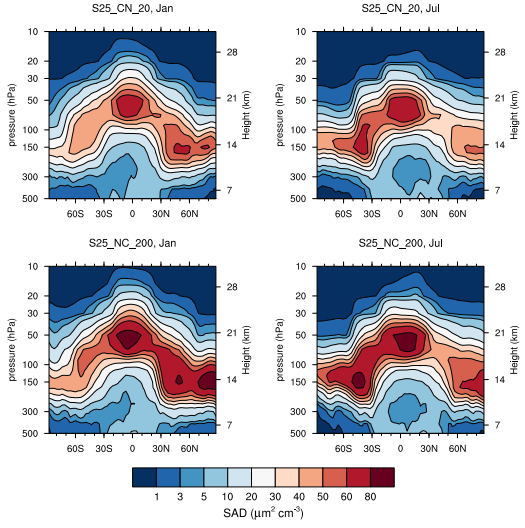

Figure S3. Same as Fig. S2, but for 25 Tg(S) yr^{-1}.

Figures S2 and S3 show the zonal mean surface area density (SAD) of sulfate aerosol for January and July. The injection of SO_2 leads to a massive increase in SAD throughout the whole lower stratosphere, with the highest SAD occurring in the polar

lowermost stratosphere, particularly during winter, and in the tropical lower stratosphere, i.e. the injection region. Figure S2 reveals substantial differences between the two S5 simulations, with S5_NC_200 showing about 20% higher SAD values, which can be explained by a 5% increase in the stratospheric aerosol burden (Table S1), combined with a shift in the size distribution towards smaller particles (Fig. 2).

S4 Influence of settings on atmospheric temperature profile

Figure S4 presents changes in the tropical temperature profile for the two SO_2 injection scenarios. The simulations show a heating of the lower stratosphere caused by the absorption of longwave radiation by the aqueous sulfuric acid aerosol, and a cooling above the aerosol layer due to reduced IR heating from below. For the S5 simulations, the maximum temperature change ranges between 4.5 and 5 K. For the S25 simulations, the warming of the lower stratosphere is much more pronounced and peaks around 15 K. For a given mass loading, the longwave absorption by sulfate aerosol does not strongly depend on the particle sizes (Lacis, 2015), so that the differences between the simulations mostly reflect differences in aerosol mass loading and its vertical distribution. The difference between the simulations increases at higher levels, reflecting the enhanced upward transport of aerosol particles for simulations with many small, and thus lighter, particles. However, the range spanned by different microphysical settings is not sufficient to explain the inter-model spread presented in Weisenstein et al. (2022, their Fig. 10): While the modeled temperature increase in MAECHAM5-HAM was only around 2 K for 5 Tg(S) yr^{-1} injection with an aerosol burden increase smaller by about 30% compared to SOCOL-AER, CESM2 showed a similar warming as SOCOL-AER, despite simulating a 50% higher aerosol burden increase.

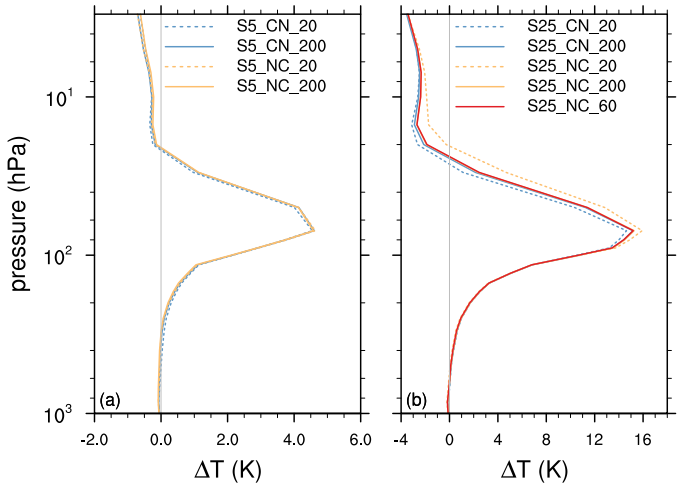

Figure S4. Change in atmospheric temperature (K) averaged between 30°S and 30°N due to SO_2 gas injections of (**a**) 5 $\mathrm{Tg(S)\,yr^{-1}}$, and (**b**) 25 $\mathrm{Tg(S)\,yr^{-1}}$. The simulation BG_CN_20 is used as reference.

As discussed in Weisenstein et al. (2022), the stratospheric warming could lead to a strengthening of the Brewer–Dobson circulation, which in turn might enhance the transport of H_2O into the stratosphere. The actual amount of H_2O entering the stratosphere, however, is largely controlled by the temperature at the tropical cold point tropopause ($\sim$ 90 hPa). As Fig. S4 does not indicate any significant differences in the simulated temperature changes at the cold point tropopause, we do not expect an influence of the settings on the modeled changes in stratospheric H_2O concentrations.

References

Lacis, A.: Volcanic aerosol radiative properties, Past Global Changes Magazine, 23, 50–51, https://doi.org/10.22498/pages.23.2.50, 2015.

Weisenstein, D. K., Visioni, D., Franke, H., Niemeier, U., Vattioni, S., Chiodo, G., Peter, T., and Keith, D. W.: An interactive stratospheric aerosol model intercomparison of solar geoengineering by stratospheric injection of SO_2 or accumulation-mode sulfuric acid aerosols, Atmos. Chem. Phys., 22, 2955–2973, https://doi.org/10.5194/acp-22-2955-2022, 2022.